Research, Society and Development, v. 12, n. 11, e96121143625, 2023
(CC BY 4.0) | ISSN 2525-3409 | DOI: http://dx.doi.org/10.33448/rsd-v12i11.43625

# Study of influence of iron, phosphorus, potassium, tantalum and fluorine on the properties of $TiNb_2O_7$

## Estudo da influência do ferro, fósforo, potássio, tântalo e flúor nas propriedades do $TiNb_2O_7$

## Estudio de la influencia del hierro, fósforo, potasio, tantalio y flúor sobre las propiedades del $TiNb_2O_7$

Received: 10/07/2023 | Revised: 10/24/2023 | Accepted: 10/29/2023 | Published: 10/31/2023

**Marco Antonio Gonçalves**
ORCID: https://orcid.org/0009-0006-3709-7610
Universidade de Uberaba, Brazil
E-mail: marco.gon430@gmail.com
**Alexandre de Faria Lima**
ORCID: https://orcid.org/0000-0002-8881-6199
Universidade de Uberaba, Brazil
E-mail: alexandredefarialima@gmail.com
**David Maikel Fernandes**
ORCID: https://orcid.org/0000-0003-3627-8998
Instituto Federal de Minas Gerais, Brazil
E-mail: davidmaikel@hotmail.com
**Rogerio Valentim Gelamo**
ORCID: https://orcid.org/0000-0003-2124-3450
Universidade Federal do Triangulo Mineiro, Brazil
E-mail: rogerio.gelamo@uftm.edu.br

**Abstract**
Recently, niobium-based oxides have attracted increasing interest as a potential choice for lithium-ion battery technology. The mixed oxide of niobium and titanium, in the composition of $TiNb_2O_7$, has been considered a promising candidate for the anodic materials of new generation lithium-ion batteries. However, its precursors require a severe and costly purification process since they are processed from complex ores. In addition to the purification cost, these steps result in significant amounts of acid and alkaline effluents, which generate additional costs for their treatment. The present research was designed to understand the influence of contaminants commonly found in ores or inserted in the process routes to obtain niobium oxides. Iron, potassium, phosphorus, tantalum, and fluoride were inserted into the $TiNb_2O_7$ synthesis process from ultrapure solutions. The mixed oxides obtained were subjected to characterizations by the X-ray diffraction technique, scanning electron microscopy and finally, applied to lithium-ion batteries to evaluate the influence on the electrochemical performance. The results showed that, despite the impact on the formation of the compound $TiNb_2O_7$, the presence of iron up to 2,000 ppm in the synthesis was not harmful to the process in general, while the presence of phosphorus and potassium resulted in serious problems in the electrode preparation steps. On the other hand, the presence of tantalum promoted important increases in battery performance, attributed to the formation of high purity mixed oxides ($TiNb_2O_7$ and $TiTa_2O_7$).
**Keywords:** Lithium-ion batteries; Hydrothermal synthesis; Niobium oxide; Mixed titanium-niobium oxide; Mixed titanium-tantalum oxide.

**Resumo**
Recentemente, os óxidos à base de nióbio têm atraído crescente interesse como uma escolha potencial para a tecnologia de baterias de íons de lítio. O óxido misto de nióbio e titânio, na composição do $TiNb_2O_7$, tem sido considerado um candidato promissor para os materiais anódicos de baterias de íons de lítio de nova geração. Entretanto, seus precursores requerem um severo e oneroso processo de purificação, uma vez que são processados a partir de minérios complexos. Além do custo de purificação, essas etapas resultam em quantidades significativas de efluentes ácidos e alcalinos, que geram custos adicionais para seu tratamento. A presente pesquisa foi idealizada para compreender a influência dos contaminantes comumente encontrados nos minérios ou inseridos nas rotas de processo para obtenção dos óxidos de nióbio. O ferro, potássio, fósforo, tântalo e flúor, foram inseridos no processo de síntese do $TiNb_2O_7$, a partir de soluções ultrapuras. Os óxidos mistos obtidos foram submetidos a caracterizações pela técnica de difração de raios X, microscopia eletrônica de varredura e, finalmente, aplicados em baterias de íon lítio para a avaliação da influência no desempenho eletroquímico. Os resultados mostraram que, apesar do impacto na formação do composto, a presença de ferro até 2.000 ppm na síntese não foi prejudicial ao processo em geral, enquanto a presença de fósforo e potássio resultou em sérios problemas nas etapas de preparação dos eletrodos. Já a presença de

tântalo promoveu aumentos importantes no desempenho da bateria, atribuídos à formação de óxidos misto de alta pureza ($TiNb_2O_7$ e $TiTa_2O_7$).
**Palavras-chave:** Baterias de íons lítio; Síntese hidrotérmica; Óxido de nióbio; Óxido misto de nióbio e titânio; Óxido misto de nióbio e tântalo.

**Resumen**

Recientemente, los óxidos a base de niobio han atraído un interés creciente como una opción potencial para la tecnología de baterías de iones de litio. El óxido mixto $TiNb_2O_7$ se ha considerado un candidato prometedor para materiales anódicos. Sin embargo, sus precursores requieren un costoso proceso de purificación, ya que se procesan a partir de minerales complejos. Además del costo de la purificación, estos pasos resultan en cantidades significativas de efluentes, que generan costos de tratamiento. La presente investigación fue diseñada para comprender la influencia de los contaminantes que se encuentran comúnmente en los minerales o insertados en las rutas de proceso para la obtención de óxidos de niobio. El hierro, el potasio, el fósforo, el tantalio y el fluoruro se insertaron en el proceso de síntesis de $TiNb_2O_7$ a partir de soluciones ultrapuras. Los óxidos mixtos obtenidos se sometieron a caracterizaciones mediante la técnica de difracción de rayos X, microscopía electrónica de barrido y, finalmente, se aplicaron a baterías de iones de litio para evaluar la influencia en el rendimiento electroquímico. Los resultados mostraron que, a pesar del impacto en la formación del compuesto, la presencia de hierro hasta 2.000 ppm en la síntesis no fue perjudicial para el proceso general, mientras que la presencia de fósforo y potasio resultó en serios problemas en las etapas de preparación del electrodo. Por otro lado, la presencia de tantalio promovió importantes aumentos en el rendimiento de las baterías, atribuidos a la formación de óxidos mixtos de alta pureza ($TiNb_2O_7$ y $TiTa_2O_7$).
**Palabras clave:** Baterias de íons lítio; Síntese hidrotérmica; Óxido de nióbio; Óxido misto de nióbio e titânio; Óxido misto de nióbio e tântalo.

## 1. Introduction

Recently, in several productive sectors, we have noticed the growth in demand for energy generation and storage. However, there is concern about the generation of electricity, due to the environmental problems caused by fossil fuels, as well as the release of polluting gases such as $CO_2$, which is the main responsible for the greenhouse effect. Another factor that leads to the need to develop new energy storage technologies is the fact of the depletion of the world oil reserve and the constant variation in its price by geopolitical factors. Renewable energy can provide two-thirds of total global energy demand and contribute to reducing greenhouse gas emissions, including to limit the increase in global average surface temperature (Gielena, 2019). Thus, energy generation and storage technologies have been standing out mainly regarding the conscious consumption of electricity. It is in this context of energy storage that lithium-ion batteries have been receiving great attention, mainly due to the possibility of application in electric cars (Bruziquesi, 2019). Lithium-based materials is considered as an important anode for the needs of batteries and are already commercialized, however, these batteries show some safety problems arising from lithium dendrites. (Griffith, 2020). Several materials are cited for application in anodes, such as graphite (Lin, 2016), lithium oxide and titanium, in the compound $Li_4Ti_5O_{12}$ (Zhao, 2015), and silicon oxide-based materials ($SiO_x$). Although silicium-based oxides have been shown to have high theoretical gravimetric capacity, silicon nanoparticles undergo rapid degradation each cycle, due to the expansion of the electrode volume of approximately 400% during lithiation, placing a large strain on the material (Anix, 2016).

In 2011, Professor Goodenough's research group (winner of the Nobel Prize in Chemistry in 2019) showed for the first time the possibility of using niobium in the form of mixed oxide with titanium as an anode material in lithium-ion batteries and aroused the interest of the scientific community in this material (Liu, 2018). Ti–Nb–O compounds, in particular, $TiNb_2O_7$, $Ti_2Nb_{10}O_{29}$ and $TiNb_{24}O_{62}$, have been considered promising candidates for the anode materials of new generation lithium-ion batteries. The attribution as promising candidates to the mixed oxides of niobium and titanium, are their more open crystal structures, which should be favorable to the mobility of lithium ions. The theoretical capacities of the mixed oxides of niobium and titanium are 388 and 396 and 402 $mAh.g^{-1}$, respectively for $TiNb_2O_7$, $Ti_2Nb_{10}O_{29}$ and $TiNb_{24}O_{62}$, and indicate the theoretical capacities twice as high as the theoretical capacity of $Li_4Ti_5O_{12}$. Ti-Nb-O compounds, in addition to having higher capacities when compared to $Li_4Ti_5O_{12}$, result in safe operations for lithium-ion batteries, not forming lithium dendrites during

the charging and discharging process (Yang, 2016), as well as showing excellent high-energy performance, fast charging, and long service life (Takami, 2018). Studies also indicate disadvantages of the compounds $Ti_2Nb_{10}O_{29}$ and $TiNb_{24}O_{62}$, when compared to $TiNb_2O_7$. The compounds with higher oxygen numbers show faulty structures which penalize them as to the stability of battery cycles. Another reason extremely important in favor of the compound $TiNb_2O_7$, as a promising substitute for $Li_4Ti_5O_{12}$, is the amount of niobium in each compound, 2:1; 5:1 and 24:1 mol of Nb:mol of Ti, respectively for the compounds $TiNb_2O_7$, $Ti_2Nb_{10}O_{29}$ and $TiNb_{24}O_{62}$. The higher dosages of Nb can make mixed oxide more expensive, making large-scale application unfeasible. However, we understand that $TiNb_2O_7$ is the compound with the greatest potential as a candidate for the replacement of $Li_4Ti_5O_{12}$, as an anode material for lithium-ion batteries (Yang, 2016).

Some methods of synthesis of $TiNb_2O_7$ are mentioned in the various literatures, however, the difficulty of obtaining raw materials or the complexity of the process route steps, may be determining factors for the success of the transfer from research scales to commercial scales. The main methods, easily found in the literature for the synthesis of mixed niobium and titanium oxide in $TiNb_2O_7$, are:

(a) Solid-state synthesis: the niobium source ($Nb_2O_5$) and the titanium source ($TiO_2$), are mixed and ground together in ball mills, with subsequent calcination in furnaces at temperatures higher than 1,000°C (Yang, 2016).

(b) Sol-gel synthesis: The source of niobium, usually niobium metal, is dissolved in hydrofluoric acid to form a transparent solution. The removal of $F^-$ ions is done from the precipitation of $Nb(OH)_5$, with ammonia. After washing and drying, the precipitate is dissolved in citric acid to form a solution of Nb (V) citrate. The titanium source, $Ti(OC_3H_7)_4$, is added to the system from the previous dissolution with water and ethanol, with pH adjustment performed with ammonia dosage. The mixture containing Nb (V) and Ti (IV) ions is heated to 90°C, under agitation until gel formation, which is treated at 900 and at 1350 °C to obtain the product $TiNb_2O_7$ (Goodenough, 2014).

(c) Solvothermal synthesis: the titanium source ($Ti(OC_3H_7)$) and the niobium source $NbCl_5$, is dissolved in absolute ethanol under vigorous agitation. The resulting solution is subjected to autoclave and kept at a temperature of 200°C for 24 hours, the precipitate obtained is washed with water and absolute ethanol and finally the precipitate is dried at 80°C, with subsequent calcination at 850°C (Yang, 2016).

Understanding the importance and potential of mixed niobium titanium oxide as a promising material in use as anode materials, regardless of the method of synthesis, the $TiNb_2O_7$ may contain impurities that come from its precursors. In the case of the niobium source, such as $Nb_2O_5$, impurities are extremely important since they are processed from complex ores and the purification process steps are the main responsible for the increase in processing cost. However, the present study was designed to understand the effect of the main impurities present in the $Nb_2O_5$ process route, such as iron, potassium, phosphorus, tantalum, and fluorine, on the physicochemical properties and electrochemical performance of the TNO, in the $TiNb_2O_7$ composition.

## 2. Methodology

The methodology applied to understand the effect of the main impurities contained in the routes of the $Nb_2O_5$ production process was the quali-quanti, which is characterized by the combination of numerical data analysis by statistical techniques that include calculations of average, standard deviation, and other statistical techniques, with the interpretation by the researcher with his opinions about the phenomenon under study. (Pereira, 2018) The methods applied in this research can be summarized in three main activities: a) the synthesis of $TiNb_2O_7$ and other compounds resulting from the presence of iron, potassium, phosphorus, tantalum, and fluorine; b) the characterization of the synthesized materials, by X-ray diffraction (XRD) and scanning electron microscopy (SEM), seeking to understand the effect of impurities on the physicochemical properties of the product and; c) the evaluation of the performance of the different materials obtained, in the application in lithium-ion

batteries of the coin-cell type, regarding the aging performance, stability and charging speed (fast charge), seeking correlations with the physicochemical properties and, consequently, the presence of impurities.

The synthesis route used in this research to obtain $TiNb_2O_7$ was developed on a laboratory scale, based on some available studies from different authors. Firstly, the choice of the niobium source was made with the premise of being a commercial niobium product. For this purpose, Niobium Ammonium Oxalate, ($NH_4[NbO(C_2O_4)_2(H_2O)](H_2O)n$), a commercial product of the Brazilian Metallurgy and Mining Company (CBMM), was chosen, which has as its main characteristic, the solubility in water of 325 g/L at 20°C, ideal for synthesis in aqueous media, as mentioned in the product portfolio of the Brazilian Company of Metallurgy and Mining (CBMM, 2020). The reagent used as a source of titanium was Titanium Oxysulfate V, from Sigma Aldrich Brasil Ltda, in 15% solution (w/v), diluted in sulfuric acid, with a purity of 99.99%. The preponderant factor in the choice of this titanium source for this synthesis was the fact that it is water soluble, which results in the optimal interaction in the synthesis methodology proposed for this research, where the raw materials were in the same physical state as the impurities studied (in solution), thus allowing the control of the insertion of impurities in a homogeneous way in the synthesis system. The synthesis of $TiNb_2O_7$ was scientifically based on sol gel synthesis, where the mixture containing Nb (V) and Ti (IV) ions was heated to 90°C, under agitation until gel formation, with subsequent treatment at 900 and 1350 °C, where the reaction in a solid state resulted in $TiNb_2O_7$ (Goodenough, 2014). The source of iron used in this study was the standard solution, at a concentration of 10,000 mg/L, from Inorganic Ventures, with a purity of 99.99%. The effect of potassium was studied from controlled dosages of 10,000 mg/L potassium nitrate solution, with a purity of 99.999%, from Inorganic Ventures Company. The study of the effect of phosphorus was carried out using the standard solution 10,000 mg/L, from SCP SCIENCE, with a purity of 99.99%. The tantalum solution was prepared in the laboratory, from the digestion of 1.0 g of Tantalum V Oxide ($Ta_2O_5$), with a purity of 99.99%, from Sigma-Aldrich, in 40 mL of acid solution, containing 10 mL of 48% hydrofluoric acid, from Merck KgAa Company, 10 ml of hydrochloric acid 37% PA, from the company Química Moderna, 10 mL of 65% Merck KGAa nitric acid and 10 mL of ultrapure water, previously treated in a Merck Millipore purifier. The solution concentration was adjusted in a volumetric flask with ultrapure water. Fluoride was studied from controlled dosages of 48% hydrofluoric acid, purchased by Merck KGaA Company.

The synthesis of mixed oxide of niobium and titanium was prepared from the dissolution of 132 g of Niobium Ammonium Oxalate (28.116 g of $Nb_2O_5$ equivalent), in 140 mL of water previously heated to 70°C, under continuous agitation. Titanium was inserted from 67.17 mL of 15% w/v Titanium Oxysulfate, containing the mass of 6.847g of Titanium Dioxide ($TiO_2$) equivalent. The addition of the impurities under study was prepared from the collection of the desired aliquot, with the use of graduated beaker and micropipette. The solution containing the components of the synthesis was kept under hot stirring until complete evaporation of the liquid phase of the solution. After complete evaporation of the aqueous phase, the precipitate underwent calcination at 1,000°C in a muffle-type furnace for the formation of the mixed oxide of niobium and titanium ($TiNb_2O_7$). The synthesis of $TiNb_2O_7$ occurred in the solid-state reaction of $Nb_2O_5$ and $TiO_2$, under a temperature of 1000°C (Yang, 2016). The procedure for the synthesis of Mixed Niobium Titanium Oxide is illustrated in Figure 1.

During the synthesis steps under high temperature the sulfuric acid contained in the $TiOSO_4$ solution, underwent the thermochemical process, that is, it underwent chemical reaction due to the exchange of energy with the external environment until there is thermal equilibrium, promoting the generation of $SO_2$ and $O_2$ gases and in this case generated water left the system in the steam form, as shown in the following equation.

$$2\ H_2SO_{4(l)} \rightarrow 2\ SO_{2(g)} + 2\ H_2O_{(l)} + O_{2(g)}$$

The titanium oxysulfate underwent the hydrolysis reaction for $TiO_2$ precipitation when subjected to temperature. All

the gases from the reactions are exhausted in the synthesis system, as well as the water contained, in the form of steam and conducted to a gas scrubber system. The reaction is proposed below in 2 reactional steps (Wahyuningsih, 2017).

$$2\ TiOSO_{4(l)} + 4\ H_2O_{(l)} \rightarrow 2\ TiO(OH)_{2(s)} + 2\ H_2O_{(l)} + 2\ SO_{3(g)}$$

$$TiO(OH)_{2(s)} \rightarrow TiO_{2(s)} + H_2O_{(l)}$$

In the following equation is shown the decomposition reaction of Niobium and Ammonium Oxalate (Medeiros, 2002). The decomposition occurred under temperature, producing ammonia ($NH_3$), carbon monoxide (CO), carbon dioxide ($CO_2$) and water, which at synthesis temperature were removed from the reaction system in the form of steam.

$$2[(NH_4)_3NbO(C_2O_4)3H_2O]_{(s)} \rightarrow (Nb_2O_5)_{(s)} + 6NH_{3(g)} + 6CO_{(g)} + 6CO_{2(g)} + 5H_2O_{(l)}$$

Finally, the reaction between $Nb_2O_5$ and $TiO_2$ occurs (Goodenough, 2014), as shown below:

$$Nb_2O_{5(s)} + TiO_{2(s)} \rightarrow TiNb_2O_{7(s)}$$

**Figure 1 -** Illustration of the synthesis procedure of mixed niobium and titanium oxide.

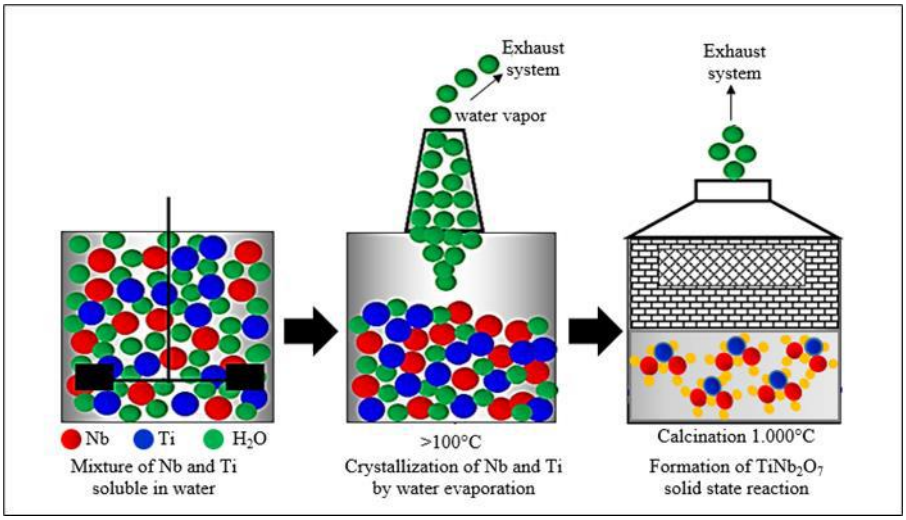


Figure 1 shows the simplified method for the $TiNb_2O_7$ synthesis, without the need for complex reactants or pressure reaction.
Source: Authors.

After the theoretical determination of the mass yield of $TiNb_2O_7$, the addition of impurities was performed, with the objective of inserting in the synthesis the amounts of contaminants as shown in Table 1.

**Table 1 -** The amount of impurities inserted during the $TiNb_2O_7$ synthesis process.

| Fe (ppm) | K (ppm) | P (ppm) | Ta (ppm) | F (ppm) |
|---|---|---|---|---|
| 2000 | 600 | 200 | 200 | 100 |
| 2.000 | 6.000 | 2.000 | 2.000 | 1.000 |
| 20.000 | 60.000 | 20.000 | 20.000 | 10.000 |

Source: Authors.

The X-ray diffraction analyses were performed by the powder method in a Bruker D8 Advance diffractometer operating with CuKα radiation and position-sensitive Lynxeye XE detector. The collection of the diffractograms was performed in the interval of 10 to 70°, and in this interval a total reading of 3080 steps was obtained, being the time/step of 0.4 seconds and the increment used of 0.02°. The identification of crystalline phases was performed by comparing the diffractograms with the PDF-4 + database of the ICDD (International Center for Diffraction Data) using the DiffracEva software and semi-quantification via the RIR (Relative Intensity Ratio) method.

Particle quality is extremely important for battery materials, nanoparticles improve connectivity between microparticles, thus improving battery performance. (Lou, 2008), nanosized particles can also increase the efficient contact between the electrode material and the electrolyte, as well as shorten the diffusion distance of lithium ions, leading to an improvement in battery capacity. $TiNb_2O_7$ synthesized with particle sizes between 50 and 300 nm, have a surface area 2.35 times larger, when compared to $TiNb_2O_7$, with particle size between 0.5 and 1 μm (Aghamohammadi, 2022). However, particle size reduction has a limitation, as extremely small particles have a negative effect on performance (Bläubaum, 2020). The scientific challenge is to determine the optimal particle size distribution for each lithium-ion battery technology (Weiss, 2021). Due to the importance of particle quality for batteries apllication, the morphologies of the particles were analyzed by Scanning Electron Microscopy (SEM), in equipment model QUANTA 450, produced by TERMO FISHER,™ coupled to an EDS (Energy Dispersive Spectroscopy) system of EDAX-AMETEK™.

The evaluation of the $TiNb_2O_7$ samples, synthesized in this work, as well as the effect of the respective contaminants, inserted in the synthesis, were evaluated with tests of charges and discharge in coin-cell type batteries, in half-cell configuration. Many are the factors that interfere in the characteristics and performance of a battery, each producing company or each researcher, has its particularities to solve problems such as different chemical systems, additives, form factors and dimensions, which will have an effect on the performances and uses of batteries (Barcellona, 2015). Therefore, the methods used for the evaluation of the synthesized samples were standardized for all samples, with the objective that the method does not interfere with the result, especially in the electrochemical measurements. The slurry preparation was done in a centrifugal mixer, of the brand: Thinky (USA), model AR-100. The slurry preparation was carried out from the mixture of the dry materials, which are the active material, in this case $TiNb_2O_7$, with the conductive agent (acetylene black, Denka Black, Denka Company Ltd, Japan), and the binder (polyvinyl fluoride, KF Polymer W#9300, Kureha, Japan), used to bind the paste. These components were added in the ratio of 8:1:1, respectively, by mass. After mixing the solids, the solvent N-methylpyrrolidone (Organics, Japan) was gradually added and mixed, until a final proportion of 38% solids, by mass, where the paste is obtained. After the preparation of the paste, the collector was coated, followed by pressing in a roller-type equipment of the brand Tester Sangyo (Japan), model: PI-1210. The height of the blade of this applicator was adjusted so that the coatings have a surface density of approximately 85 g/m$^2$. The coated collectors were dried in a vacuum oven of the brand Yamato Scientific Co (Japan), model DP610P, at 120 °C for 15 hours. The resulting electrodes were pressed in a double cylinder calender type press, with the objective of adjusting the coatings to a density of approximately 2.1 g/cm$^3$. To assemble the cell, the electrode was cut, in a diameter of 12 mm, in a manual cutter of the brand Hohsen Corp. (Japan), impregnated in the electrolytic solution (1 mol/L-1 LiPF6 EC:DEC 1:1 v/v, Chameleon, Japan) for 30 min. The final mass of active material ($TiNb_2O_7$) in the electrode already cut was of the order of 7.4 to 7.9 mg. The cell was assembled by positioning its components (cathode base, seal, TNO electrode, polyethylene film separator, electrolyte solution, lithium electrode, spacer, washer and anode base), and sealed. The entire procedure of mounting the battery was done in argon atmosphere in glove box of the brand Miwa Mfg Co (Japan), model DBO-2BL. The electrochemical measurements of the coin-type batteries were performed in equipment of the brand Toyo System Co. (Japan), model Toscat-3100. Through electrochemical measurements, we can understand among other characteristics of the battery the fast charging, currently seen as a crucial characteristic for electric vehicles, however, the

battery capacity usually decreases rapidly if the batteries are charged in severe conditions, so the combination of shorter charging time with higher capacities is an important prerequisite of lithium-ion batteries (Hu, 2021).

## 3. Results and Discussion

The results obtained from the analyses by the X-ray diffraction method showed that the synthesis resulted in the mixed oxide of niobium and titanium of high phase purity in $TiNb_2O_7$. The presence of 200 ppm of iron, promoted the imbalance in the synthesis of $TiNb_2O_7$, also promoting the formation of the mixed oxide $Ti_2Nb_{10}O_{29}$ and $TiO_2$, this effect was potentiated with the addition of 2,000 ppm of iron. The results obtained, with the presence of 20,000 ppm of iron, promoted in addition to the imbalance of synthesis, with the formation of the mixed oxide of niobium and titanium in stoichiometry of $Ti_2Nb_{10}O_{29}$, synthesized the mixed oxide of $Ti_{0.78}Nb_{0.11}Fe_{0.11}O_2$. The imbalance of $TiNb_2O_7$ synthesis with the presence of iron can be explained by the high reactivity of iron and titanium, potentiated above 400 ºC in the presence of $O_2$. This high reactivity of titanium and iron, in the presence of oxygen, under temperature, is the reason why they are commonly found in the Earth's crust in the form of titanium dioxide and in the various combinations of iron oxides (Bragal, 2007). The increasing presence of potassium in the synthesis process, reduced the formation of $TiNb_2O_7$ and increased the formation of $Ti_2Nb_{10}O_{29}$ and $TiO_2$, the results obtained showed that the increase in potassium interferes in the stoichiometric balance of $TiNb_2O_7$ formation. Already in high quantities (60,000 ppm), this interference was evident, and it was not possible to identify the compounds formed, with the use of the database of PDF-4+ of the ICDD (International Center for Diffraction Data). The presence of phosphorus, in the order of 200 and 2,000 ppm, promoted the reaction imbalance of the synthesis, forming the compound $Ti_2Nb_{10}O_{29}$, and $TiO_2$. Phosphorus at 20,000 ppm resulted in reduced formation of $Ti_2Nb_{10}O_{29}$ and $TiO_2$, and synthesized mixed oxides of niobium and phosphorus, such as $NbPO_5$ and $Nb_9PO_{25}$. The studies of the influence of tantalum, in synthesis with niobium, are very delicate since the characteristics of these two important elements are quite similar. The presence of tantalum up to 2,000 ppm showed the interaction of the formation of mixed titanium and tantalum oxide in the stoichiometry of $TiTa_2O_7$, in addition to the formation of $Ti_2Nb_{10}O_{29}$ and $TiO_2$. The presence of 20,000 ppm potentiated the formation of mixed oxides $TiNb_2O_7$ and $TiTa_2O_7$. The results obtained by X-ray diffractograms indicate that the presence of fluoride in the $TiNb_2O_7$ synthesis system does not promote significant reaction imbalance, to the point of impairing the formation of the pure phase of $TiNb_2O_7$. The absence of fluorine in the $TiNb_2O_7$ diffractograms, shown in the images in Figure 2, can be justified by the reaction step of the synthesis occurring at a temperature of 120°C, in the precipitation step and at 1,000°C, in the solid-state reaction step, since hydrofluoric acid initiates vaporization at temperatures in the order of 19.5°C. The obtainment of the mixed oxide of niobium and titanium of high phase purity, confirms that in the conditions of synthesis of $TiNb_2O_7$, applied in this work, there is no complex formation occurred between niobium and fluorine, commonly synthesized for the processing of niobium oxide, from processing routes of ores containing high concentrations of tantalum, where hydrofluoric acid is used as a solvent and as a complexing agent, in compound $NbOF_5^{2-}$ (Rodríguez, 2020).

**Figure 2 -** Diffractograms of mixed oxides obtained in the synthesis process.

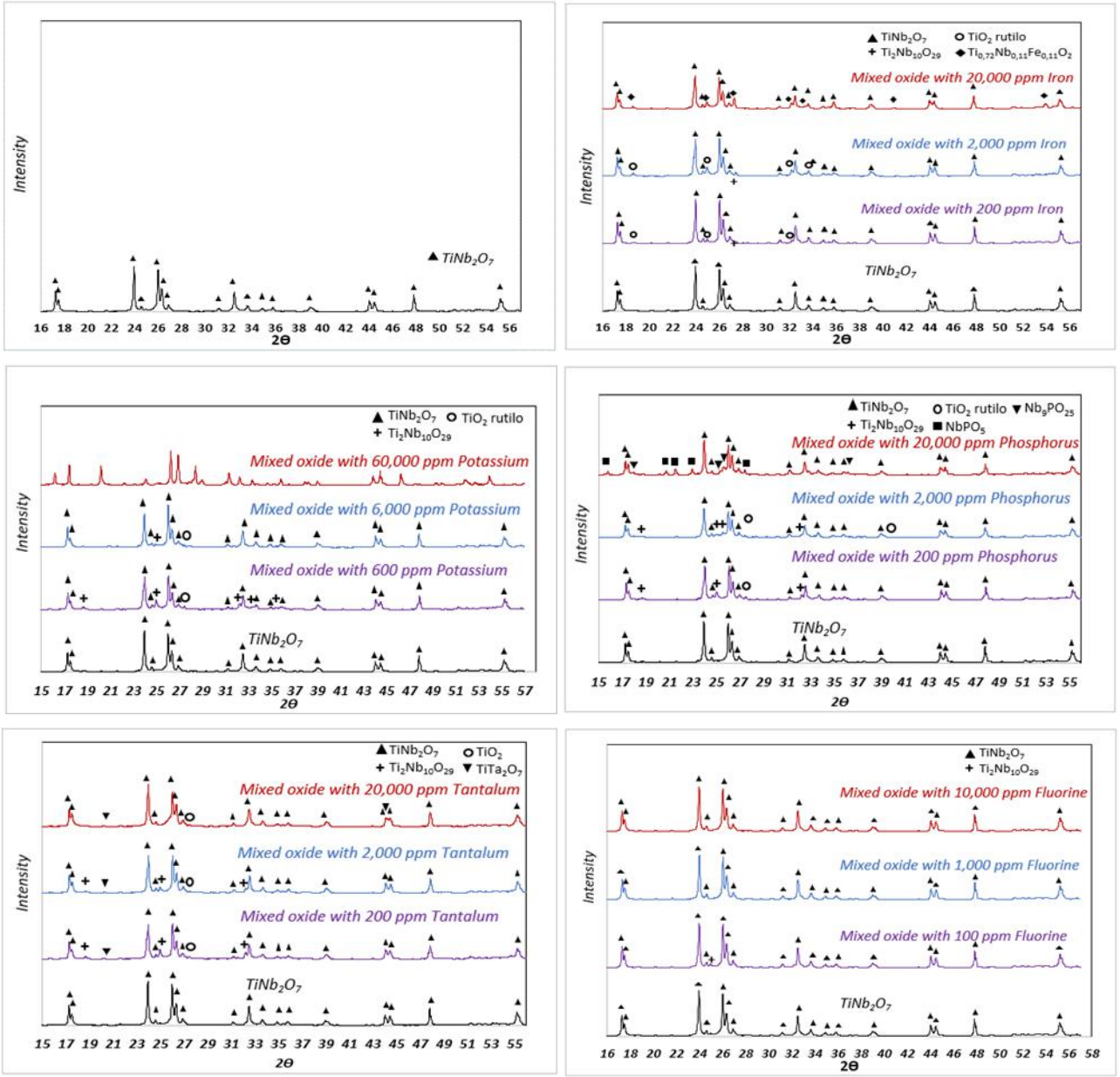


Figure 2 shows the interference of impurities in obtaining high purity mixed oxide in $TiNb_2O_7$. Source: Authors.

The results stratified by semiquantitative analyses, from the crystallographic peaks detected by X-ray diffraction, shown in Figure 3, allowed the understanding of the reactional behavior of the formation of the compounds, with the increasing presence of the impurities studied in this work.

**Figure 3 -** Results stratified by semiquantitative analyses, from the crystallographic peaks detected by X-ray diffraction.

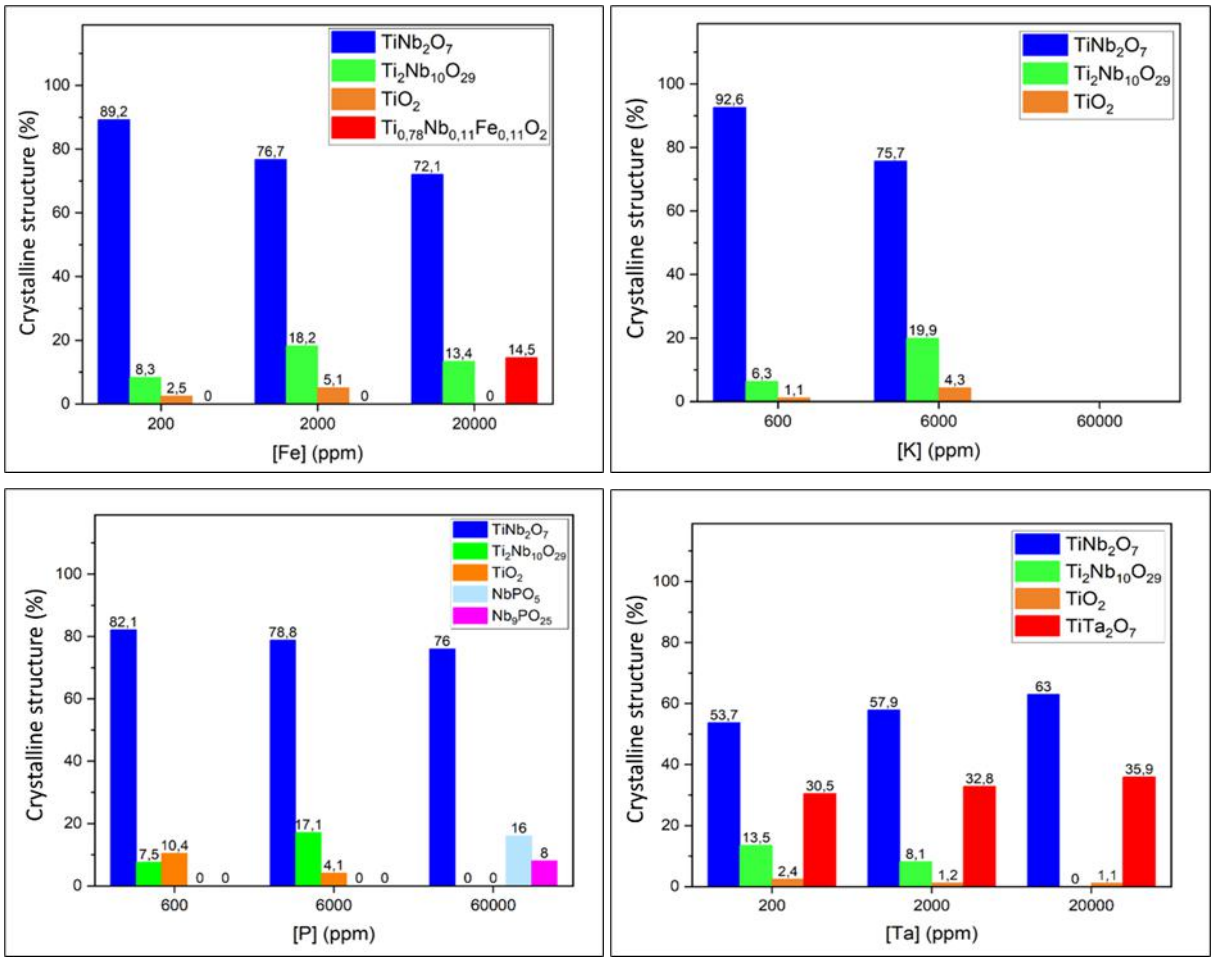


Figure 3 shows that the impurities promoted the imbalance in the $TiNb_2O_7$ formation reaction. The presence of the impurities resulted in mixed oxides with other stoichiometries. Source: Authors.

In Figure 4, we can find the results of the mapping of the impurities studied in this work by the technique of Energy Dispersive Spectroscopy (EDS). The images identified as a, b and c, which refer to the material synthesized with 200, 2,000 and 20,000 ppm of iron respectively. The increasing presence of iron can be seen in the yellow coloration and shows us the absence of severe iron agglomerations in the sample. The presence of potassium in the oxides synthesized in the order of 600 ppm (d), 6,000 ppm (e) and 60,000 ppm (f), can be seen by the green coloration. In image f, it is already possible to observe some potassium segregation in some regions of the sample. The resulting images of mixed oxides synthesized with the presence of phosphorus, identified as g (200 ppm), h (2,000 ppm) and i (20,000 ppm). In the image with the highest presence of phosphorus (i), we can find areas of phosphorus segregation. The mapping of the synthesized samples with the presence of tantalum, identified as j (200 ppm), k (2,000 ppm) and l (20,000 ppm), shows us the homogeneous presence of tantalum in yellow color in all areas of the samples. The presence of fluoride in small amounts, shown in red color in the images m (100 ppm), n (1,000 ppm) and o (10,000 ppm), can be attributed to small complexes formed between fluorine, niobium, which prevented the exit of fluorine in the gas form, during the heat treatments of the synthesis.

**Figure 4 -** Images obtained by Energy Dispersive Spectroscopy (EDS).

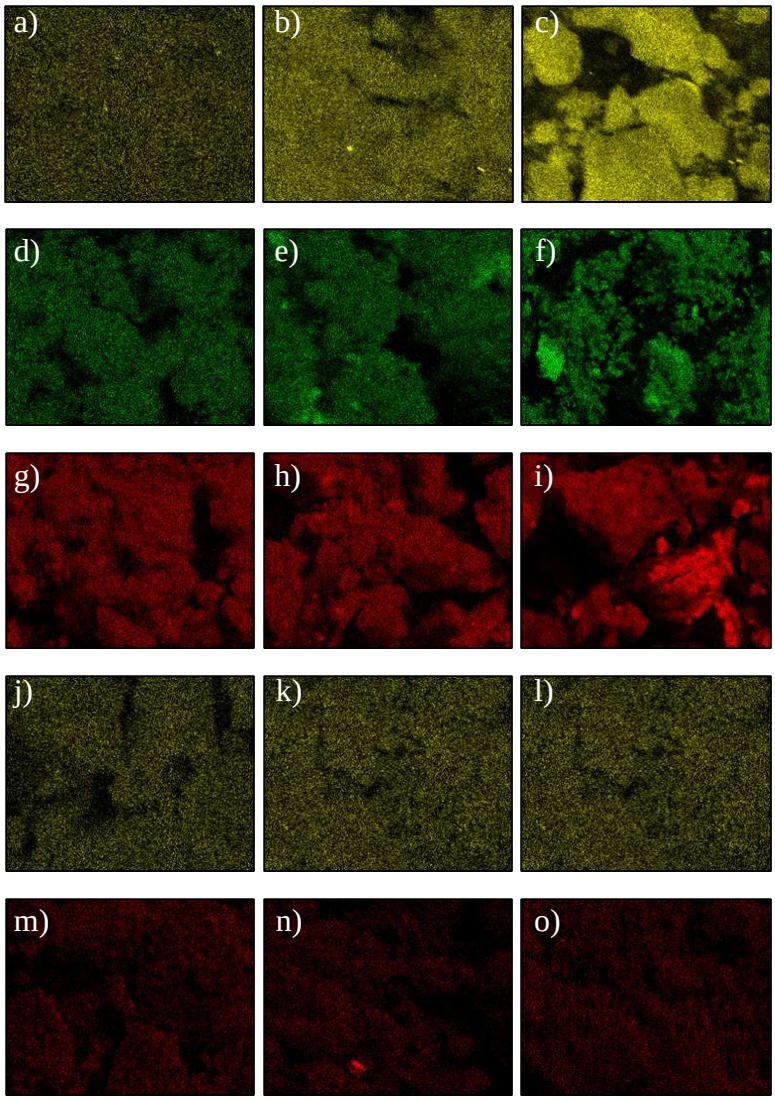


Figure 4 shows the presence of impurities inserted in the $TiNb_2O_7$ synthesis process. In the images it is possible to identify agglomerations of impurities occurring in the sampling regions. Source: Authors.

In Figure 5, we can find the results of the characterization of the mixed oxides obtained by the Optical Scanning Microscopic (SEM). Images a, b and c show us that the mixed oxide obtained of high purity in $TiNb_2O_7$, resulted in particles of high quality in terms of homogeneity. The images d, e, and f, corresponding to the material with the presence of iron at 200, 2,000 and 20,000 ppm respectively, indicate that the increasing in iron resulted in heterogeneous particle size. The images g, h and i, corresponding to the addition of 600, 6,000 and 60,000 ppm of potassium respectively and show us that the presence of potassium in the synthesis of $TiNb_2O_7$, resulted in heterogeneous and elongated particles, which may result in the need for severe grinding for use as anodic material. The images j, k and l, come from the mixed oxides obtained with the addition of 200 (j), 2,000 (k) and 20,000 ppm (l) of phosphorus and shows us that the increasing presence of phosphorus promoted severe agglomerations of the primary particles. The m and n images indicate that the presence of tantalum in the order of 200 (m) and 2,000 ppm (n) in the $TiNb_2O_7$ synthesis system did not promote significant damage to the particles, except at 20,000 ppm (image o) which showed some agglomeration. In the same way that the results obtained in the X-ray diffraction characterizations did not show significant impacts of fluorine on the formation of $TiNb_2O_7$, the images p (100 ppm), q (1,000 ppm) and r (10,000 ppm), also show us the excellent quality of the particles. Due to the results obtained from the synthesis of

TiNb2O7, with the presence of fluorine in the reaction system, to show us that this contaminant did not interfere in the synthesis or morphology of the particles, the $TiNb_2O_7$ synthesized with the presence of fluorine was not submitted to evaluation of the electrochemical potential.

**Figure 5** - Images obtained by Scanning Electron Microscopy (SEM).

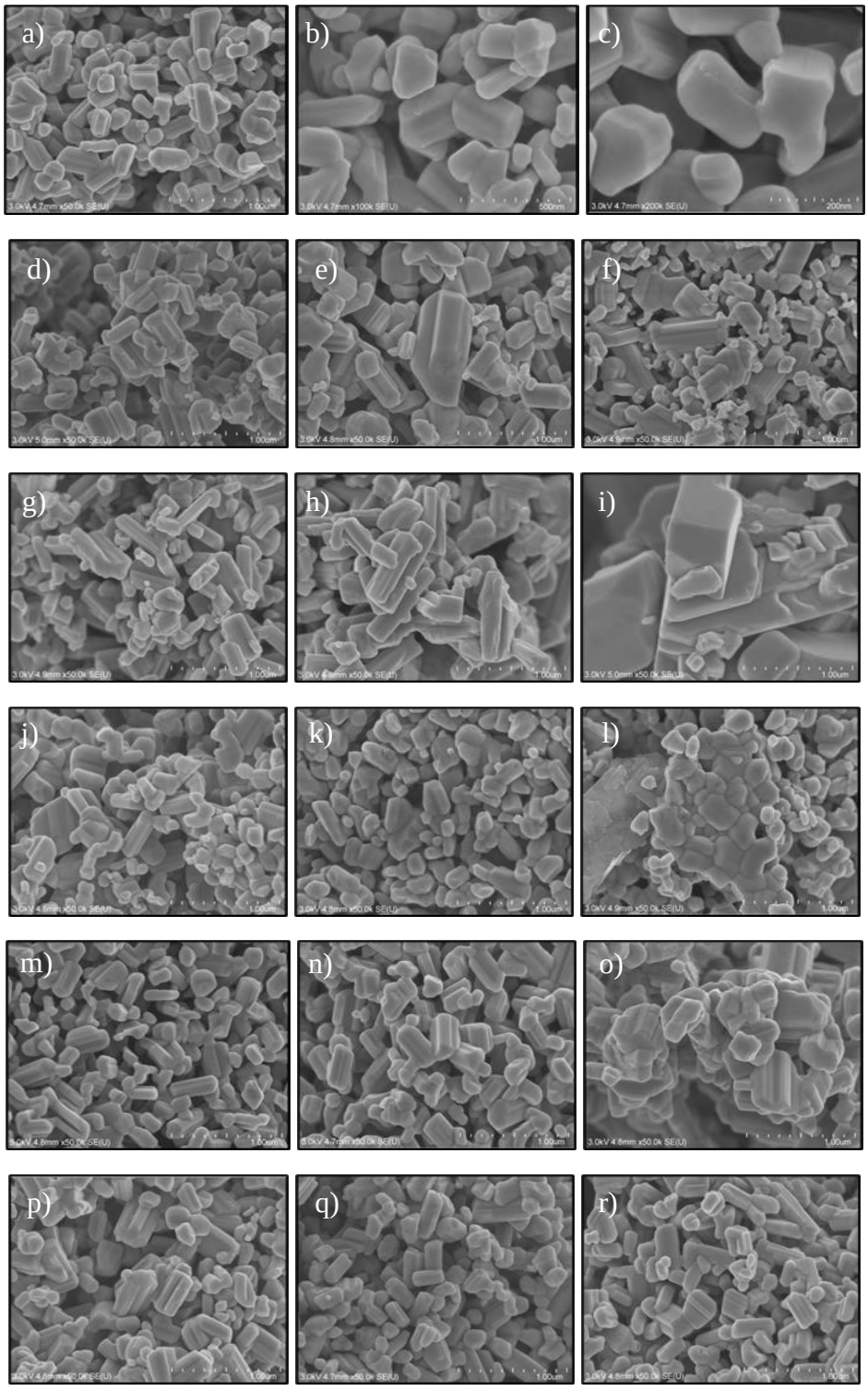


Figure 5 shows the damage to the morphological quality caused by the increasing presence of impurities, especially regarding the homogeneity and agglomeration of the particles. Source: Authors.

For the electrochemical evaluation of the battery with the use of mixed oxides synthesized as to aging, during the

battery discharge step, the applied current was 78 mA/g, with potential readings every 10 seconds, until reaching the potential limit of 1.0 V. Then, this same potential is applied with current readings every 10 seconds until the limit current is reached. In the charge step, a current of 78 mA/g was applied, and potential readings were taken every 10 seconds until the limit potential of 3.0 V was reached. The reduction in gravimetric capacity, or aging, between the first and second cycles can be attributed to the phenomenon known as Solid Electrolyte Interphase (SEI), which is a solid layer of decomposed organic solvent that forms on the first charge of the battery (Bommier, 2018). The formation of a SEI on the electrode surface is crucial for the cycle stability and durability of batteries, preventing the decomposition of the organic solvent, important in the life and durability of the battery (Wang, 2020).

Electrochemical measurements using high-purity $TiNb_2O_7$ showed average gravimetric capacities in battery discharge of 285.8 mAh.g$^{-1}$ TNO in the first cycle and 267.1 mAh.g$^{-1}$ TNO in the second cycle. The reduction in gravimetric capacity from the first to the second cycle was 6.5%. The gravimetric capacity in battery charging was 266.8 mAh.g$^{-1}$ TNO in the first cycle and 261.8 mAh.g$^{-1}$ TNO in the second cycle. The reduction of gravimetric capacity in charging between the first and second cycle was only 1.9%.

The results obtained in the battery of $TiNb_2O_7$ with additon of 200 ppm of iron, showed, in the discharge step, the average gravimetric capacity of 279.6 mAh.g$^{-1}$ TNO in the first cycle and 267.1 mAh.g$^{-1}$ TNO in the second cycle. The results obtained in the second discharge showed a reduction of 4.5% in the average gravimetric capacity. The average gravimetric capacity in battery charging was 266.9 mAh.g$^{-1}$ TNO in the first cycle and 263.5 mAh.g$^{-1}$ TNO in the second cycle. The reduction of gravimetric capacity in charging between the first and second cycle was only 1.3%. For the battery of $TiNb_2O_7$ with addition of 2,000 ppm of iron, the discharge showed an average gravimetric capacity of 285.3 mAh.g$^{-1}$ TNO in the first cycle and 275.5 mAh.g$^{-1}$ TNO in the second cycle, the gravimetric capacity reduction was 3.4% from the first to the second discharge cycle. The average gravimetric capacity in battery charging was 275.5 mAh.g$^{-1}$ TNO in the first cycle and 271.4 mAh.g$^{-1}$ TNO in the second cycle, the reduction of gravimetric capacity in charging between the first and second cycle was only 1.5%. Finally, for the battery with $TiNb_2O_7$ contaminated with 20,000 ppm of iron, the discharge showed an average gravimetric capacity of 279.4 mAh.g$^{-1}$ TNO in the first cycle and 249.9 mAh.g$^{-1}$ TNO for the second cycle, the reduction in gravimetric capacity between the first and second cycles was 10.6%. For battery charging, the average gravimetric capacity was 248.6 mAh.g$^{-1}$ TNO in the first cycle and 244.7 mAh.g$^{-1}$ TNO in the second cycle, the reduction in gravimetric capacity in charging between the first and second cycle was only 1.6%.

The average gravimetric capacity obtained with $TiNb_2O_7$ contaminated with 600 ppm of potassium in the discharge step was 279.4 mAh.g$^{-1}$ TNO in the first cycle and 266.3 mAh.g$^{-1}$ TNO for the second cycle. The results obtained in the second discharge showed a reduction of gravimetric capacity of 4.7%. The average gravimetric capacity in battery charging was 266.7 mAh.g$^{-1}$ TNO in the first cycle and 263.1 mAh.g$^{-1}$ TNO in the second cycle. The reduction of gravimetric capacity in charging between the first and second cycle was only 1.3%. For the battery with $TiNb_2O_7$ contaminated with 6,000 ppm of potassium, the discharge showed an average gravimetric capacity of 263.6 mAh.g$^{-1}$ TNO in the first cycle and 256.4 mAh.g$^{-1}$ TNO for the second cycle, the reduction of gravimetric capacity was 2.7%. The average gravimetric capacity in battery charging was 253.9 mAh.g$^{-1}$ TNO in the first cycle and 252.6 mAh.g$^{-1}$ TNO in the second cycle, the reduction of gravimetric capacity was only 0.5%. Finally, for the battery with $TiNb_2O_7$ contaminated with 60,000 ppm of potassium, average gravimetric capacity were significantly low, disqualifying the mixed oxide synthesized as anode material.

The results obtained with the $TiNb_2O_7$ battery contaminated with 200 ppm of phosphorus showed, in the discharge step, the average gravimetric capacity of 279.8 mAh.g$^{-1}$ TNO in the first cycle and 268.9 mAh.g$^{-1}$ TNO for the second cycle. The results obtained in the second discharge showed a reduction of gravimetric capacity of 3.9%. The average gravimetric capacity in battery charging was 268.5 mAh.g$^{-1}$ TNO in the first cycle and 264.4 mAh.g$^{-1}$ TNO in the second cycle. The

reduction of gravimetric capacity in charging between the first and second cycle was only 1.5%. For the battery with $TiNb_2O_7$ contaminated with 2,000 ppm of phosphorus, the discharge showed an average gravimetric capacity of 280.0 mAh.g$^{-1}$ TNO in the first cycle and 269.9 mAh.g$^{-1}$ TNO for the second cycle. The reduction of gravimetric capacity was 3.6% from the first to the second discharge cycle. The average gravimetric capacity in battery charging was 269.4 mAh.g$^{-1}$ TNO in the first cycle and 264.2 mAh.g$^{-1}$ TNO in the second cycle, the reduction of gravimetric capacity in charging between the first and second cycle was only 1.9%. Finally, for the battery with $TiNb_2O_7$ contaminated with 20,000 ppm of phosphorus, the discharge showed an average gravimetric capacity of 283.0 mAh.g$^{-1}$ TNO in the first cycle and 261.1 mAh.g$^{-1}$ TNO for the second cycle. The reduction in gravimetric capacity between the first and second cycles was 7.7%. The average gravimetric capacity in battery charging, with the presence of 20,000 ppm of phosphorus was 258.8 mAh.g$^{-1}$ TNO in the first cycle and 252.7 mAh.g$^{-1}$ TNO in the second cycle. The reduction of gravimetric capacity in charging between the first and second cycle was only 2.4%.

The results obtained for the battery with $TiNb_2O_7$ contaminated with 200 ppm of tantalum, showed, in the discharge step, the average gravimetric capacity of 278.6 mAh.g$^{-1}$ TNO in the first cycle and 267.8 mAh.g$^{-1}$ TNO for the second cycle. The results obtained in the second discharge showed a reduction of gravimetric capacity of 3.9%. The average gravimetric capacity in battery charging was 267.0 mAh.g$^{-1}$ TNO in the first cycle and 263.6 mAh.g$^{-1}$ TNO in the second cycle. The reduction of gravimetric capacity in charging between the first and second cycle was only 1.3%. For the battery with $TiNb_2O_7$ contaminated with 2,000 ppm of tantalum, the discharge showed an average gravimetric capacity of 282.8 mAh.g$^{-1}$ TNO in the first cycle and 274.3 mAh.g$^{-1}$ TNO for the second cycle. The gravimetric capacity reduction was 3.0% from the first to the second discharge cycle. The average gravimetric capacity in battery charging was 274.3 mAh.g$^{-1}$ TNO in the first cycle and 270.4 mAh.g$^{-1}$ TNO in the second cycle, the reduction of gravimetric capacity in charging between the first and second cycle was only 1.4%. Finally, for the battery with $TiNb_2O_7$ contaminated with 20,000 ppm of tantalum, the discharge showed an average gravimetric capacity of 276.7 mAh.g$^{-1}$ TNO in the first cycle and 270.9 mAh.g$^{-1}$ TNO for the second cycle. The reduction in gravimetric capacity between the first and second cycles was 2.1%. The average gravimetric capacity in battery charging, with the presence of 20,000 ppm of tantalum, was 270.4 mAh.g$^{-1}$ TNO in the first cycle and 268.4 mAh.g$^{-1}$ TNO in the second cycle. The reduction of gravimetric capacity in charging between the first and second cycle was only 0.7%. The results obtained regarding the aging of the batteries are shown in Table 2.

**Table 2 -** Evaluation of the electrochemical potential of synthesized mixed oxides for aging.

| **Added impurities** | **ppm** | **Discharge** (mAh.g$^{-1}$ TNO) | | **Charge** (mAh.g$^{-1}$ TNO) | |
|---|---|---|---|---|---|
| | | **1st cycle** | **2nd cycle** | **1st cycle** | **2nd cycle** |
| - | - | 285,8 | 267,1 | 266,8 | 261,8 |
| Fe | 200 | 279,6 | 267,1 | 266,9 | 263,5 |
| | 2.000 | 285,3 | 275,5 | 275,5 | 271,4 |
| | 20.000 | 279,4 | 249,9 | 248,6 | 244,7 |
| K | 600 | 279,4 | 266,3 | 266,7 | 263,1 |
| | 6.000 | 263,6 | 256,4 | 253,9 | 252,6 |
| | 60.000 | 46,9 | 22,6 | 17,4 | 17,2 |
| P | 200 | 279,8 | 268,9 | 268,5 | 264,4 |
| | 2.000 | 280,0 | 269,9 | 269,4 | 264,2 |
| | 20.000 | 283,0 | 261,1 | 258,8 | 252,7 |
| Ta | 200 | 278,6 | 267,8 | 267,0 | 263,6 |
| | 2.000 | 282,8 | 274,3 | 274,3 | 270,4 |
| | 20.000 | 276,7 | 270,9 | 270,4 | 268,4 |

Source: Authors.

The electrochemical evaluations of the batteries for stability, at charge of 1C, with the use of $TiNb_2O_7$ without the addition of contaminants, showed the reduction of accumulated gravimetric capacity of 52.1 mAh.g$^{-1}$ TNO (22.0%) in the 13th cycle, 77.5 mAh.g$^{-1}$ TNO (32.7%) in the 23rd cycle, 110.5 mAh.g$^{-1}$ TNO (42.5%) in the 33rd cycle, 121.5 mAh.g$^{-1}$ TNO (51.3%) in the 43rd cycle and finally in the 53rd cycle the cumulative reduction in battery discharge reached 137.1 mAh.g$^{-1}$ TNO (57.9%).

The results of battery discharge, with the presence of 200 ppm of iron, indicate the gravimetric capacity of 261.3 mAh.g$^{-1}$ TNO in the discharge of the 3rd cycle and the gravimetric capacity of 168.5 mAh.g$^{-1}$ TNO in the 53rd cycle, a cumulative reduction of 35.5%. The battery capacity with the mixed oxide containing 2,000 ppm of iron showed discharge capacity of 267.6 mAh.g$^{-1}$ TNO in the 3rd cycle and 122.3 mAh.g$^{-1}$ TNO in the 53rd cycle, a cumulative reduction of 40.4%. The mixed oxide with the highest amount of iron (20,000 ppm), showed gravimetric capacity of 251.9 mAh.g$^{-1}$ TNO in the 3rd cycle, compared to the discharge capacity of 111.1 mAh.g$^{-1}$ TNO in the 53rd cycle, accumulating a reduction of 55.9%.

The battery discharge results obtained, with the presence of 600 ppm of potassium were 259.3 mAh.g$^{-1}$ TNO in the discharge of the 3rd cycle and 149.5 mAh.g$^{-1}$ TNO in the discharge 53rd cycle, accumulated reduction of 42.3%. The discharge capacity of the battery with the mixed oxide containing 6,000 ppm of potassium showed discharge capacity of 237.4 mAh.g$^{-1}$ TNO in the 3rd cycle and 151.2 mAh.g$^{-1}$ TNO in the 53rd cycle, 36.5% reduction of accumulated gravimetric capacity.

The battery discharge measurements, with the presence of 200 ppm of phosphorus in the anode material showed the gravimetric capacity of 251.2 mAh.g$^{-1}$ TNO in the discharge of the 3rd cycle and 115.9 mAh.g$^{-1}$ TNO in the discharge 53rd cycle, reduction of 146.1%. The battery capacity with the mixed oxide containing 2,000 ppm of phosphorus showed discharge capacity of 246.4 mAh.g$^{-1}$ TNO in the 3rd cycle and 122.8 mAh.g$^{-1}$ TNO in the 53rd cycle, reduction of 50.2%. The mixed oxide with the highest amount of phosphorus (20,000 ppm), showed gravimetric capacity of 242.2 mAh.g$^{-1}$ TNO in the 3rd cycle, compared to the discharge capacity of 134.1 mAh.g$^{-1}$ TNO in the 53rd cycle, capacity reduction of 44.6%.

The presence of 200 ppm of tantalum in the anode material showed battery stability values during discharge in the 3rd cycle of 247.7 mAh.g$^{-1}$ TNO and 117.5 mAh.g$^{-1}$ TNO in the 53rd cycle, thus reducing gravimetric capacity in.6%. The presence of tantalum at 2,000 ppm resulted in discharge values of 256.3 mAh.g$^{-1}$ TNO in the 3rd cycle and 100.2 mAh.g$^{-1}$ TNO in the 53rd cycle, 60.9% capacity reduction. The presence of tantalum at 20,000 ppm in the active material resulted in the capacity of 262.4 mAh.g$^{-1}$ TNO in the 3rd cycle compared to 176.3 mAh.g$^{-1}$ TNO in the 53rd cycle, so the cumulative capacity reduction was 32.8%. In Figure 6, we can observe the evolution of the gravimetric capacity obtained in the stability evaluations of the batteries.

**Figure 6 -** Evolution of gravimetric capacity of battery discharge, regarding the stability from 3 to 53 cycles.

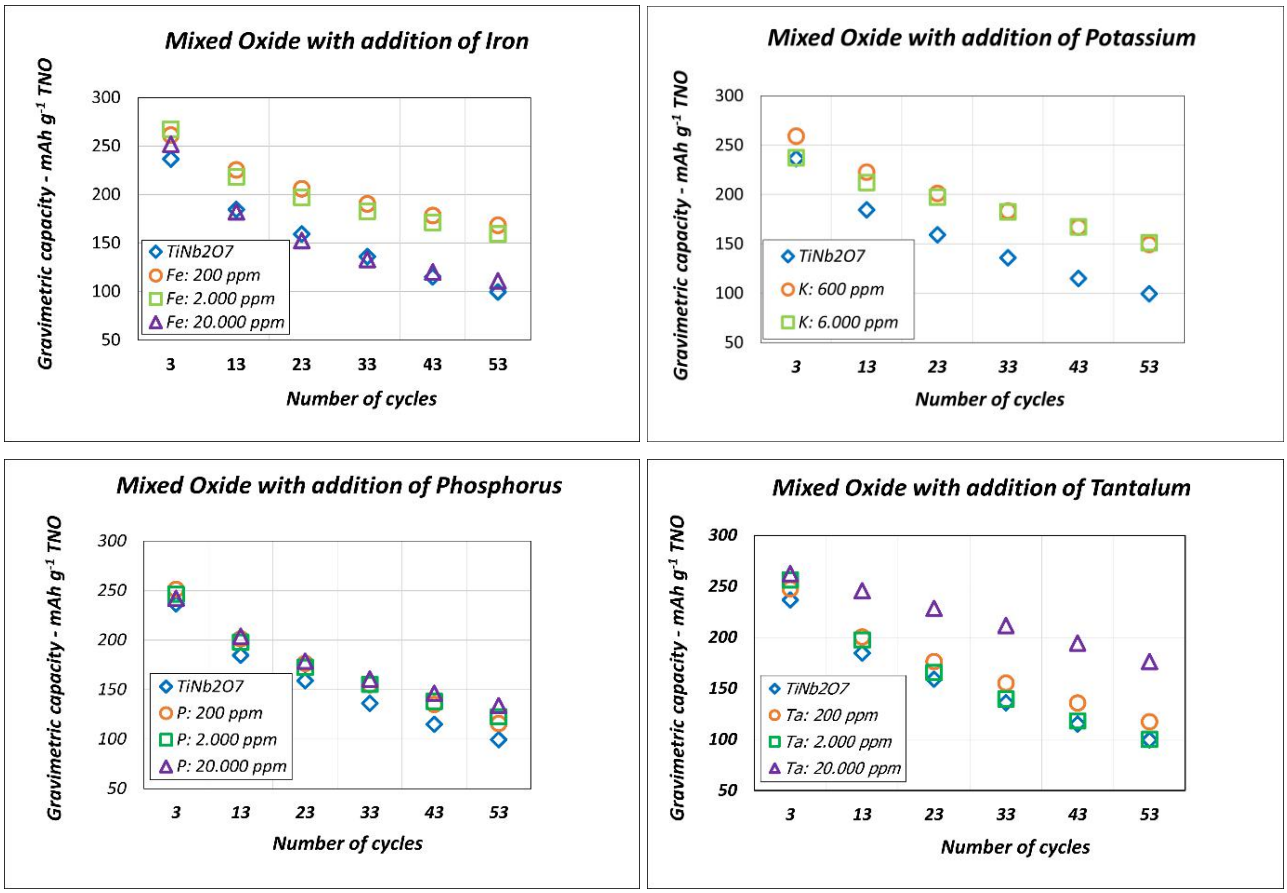


Figure 6 shows the impact of each impurity under study on battery performance in up to 53 cycles. We can also observe the significant increase in battery performance with the increasing presence of tantalum in the synthesized mixed oxide. Source: Authors

To conclude the evaluation of the batteries with the use of mixed oxides synthesized in this work, the measurements of discharges and charges were performed in three repetitions, at the charging of 0.2C (300 minutes), 1C (60 minutes), 2C (30 minutes), 3C (20 minutes) and 5C (12 minutes).

At the slowest charge applied to the battery (0.2C) with the use of high-purity $TiNb_2O_7$, the discharge capacity was 258.4 mAh/$g^{-1}$ TNO. When the battery was charged at 1C, the gravimetric discharge capacity was 245.6 mAh/$g^{-1}$ TNO, 5% smaller than the same battery charged more slowly. The charge of 2C showed an average result of 237.7 mAh/$g^{-1}$ TNO, 8.0% lower than the results obtained with the slower charge of 0.2C. When we charged the battery in 3C, the gravimetric discharge capacity was 229.4 mAh/$g^{-1}$ TNO, 11.2% lower when compared to the 0.2C charge. The fastest charge that the battery was submitted, 5C, showed gravimetric discharge capacity of 217.4 mAh/$g^{-1}$ TNO, 15.9% lower when compared to the slower charge of 0.2C.

The results obtained in the evaluations regarding the speed of battery charge with the presence of iron in $TiNb_2O_7$, showed that the presence of iron up to 2,000 ppm, increased the gravimetric capacity of the discharge by 7.9% (234.6 mAh/$g^{-1}$ TNO) when compared with the results obtained with TiNb2O7 of high purity. The presence of 20,000 ppm of iron in the anode material showed results similar to those obtained with high-purity $TiNb_2O_7$.

The results obtained with the presence of 600 ppm of potassium in the anode material showed that the discharge capacity in 5C of 9.4% higher (237.8 mAh/$g^{-1}$ TNO) than the $TiNb_2O_7$ of high purity, while the results with the presence of 6,000 ppm of potassium showed results in 5C, 2.8% higher (223.5 mAh/$g^{-1}$ TNO) than the anode material of high purity.

The presence of phosphorus up to 2,000 ppm in the anode material was 4.7% higher (227.7 mAh/$g^{-1}$ TNO) than the

results obtained with the high purity mixed oxide and 5.8% higher (230.1 mAh/g$^{-1}$ TNO) than the results with the presence of 20,000 ppm of phosphorus.

The best results obtained regarding the speed of charging the battery in 5C, was with the presence of tantalum in the anodic material, the results showed an increase of 3.1% (224.2 mAh/g$^{-1}$ TNO) with the presence of 200 ppm, 10.7% (240.6 mAh/g$^{-1}$ TNO) with the presence of 2,000 ppm of tantalum and 17.9% (256.3 mAh/g$^{-1}$ TNO) of increase with the presence of 20,000 ppm of tantalum in the anodic material.

In Figure 7, we can find the results of the electrochemical evaluations of the batteries regarding the charging speeds, carried out with the mixed oxides synthesized in this study.

**Figure 7 -** Results of electrochemical evaluations of batteries at different charging speeds.

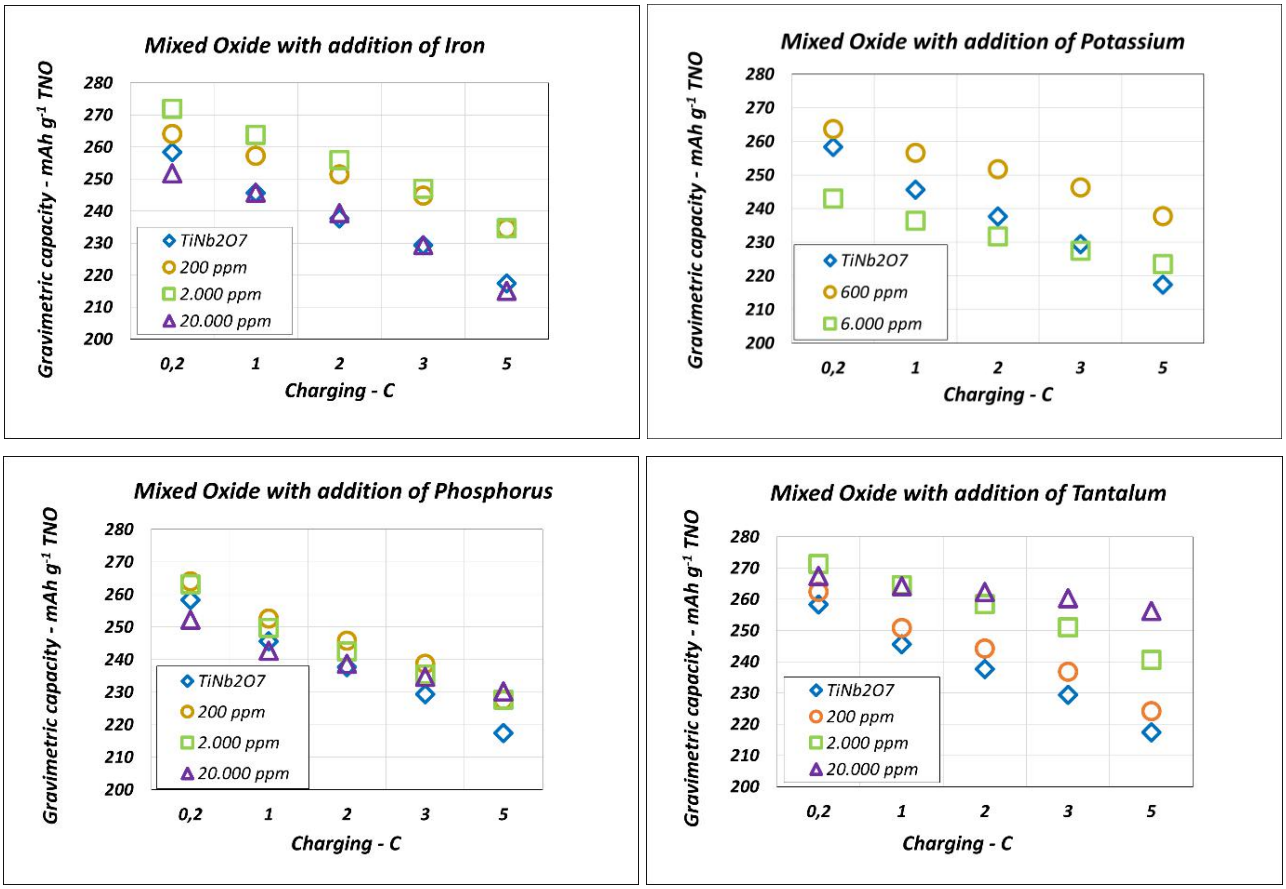


Figure 7 shows the impact of each impurity under study on the preliminary battery performance in terms of fast charge capacity. We can also observe the significant increase in battery performance with the presence of tantalum Source: Authors.

## 4. Conclusion

The results obtained in this research allow us to conclude that it is possible to synthesize the mixed oxide of niobium and titanium, in the compound $TiNb_2O_7$ of high purity, with high morphological quality of the particles, as to the homogeneity of sizes and shapes, through a simplified synthesis route, where high pressures or complex reagents are not applied. However, the limiting factor for an industrial scaling may be the cost and supply of the titanium source in solution, such as Titanium Oxysulfate V. Despite the impact on the formation of high-purity $TiNb_2O_7$, the presence of iron up to 2,000 ppm in the synthesis system showed that it can be positive in the process in general, may promote increased battery performance, attributed to increased conductivity in the active material. The positive impact of iron also contributes to the potential reduction

of purification costs in the production process of the precursors of synthesis. The significant increase in the presence of iron in the synthesis results in the formation of the mixed oxide of titanium, niobium and iron ($Ti_{0.78}Nb_{0.11}Fe_{0.11}O_2$), resulting in heterogeneous particles and consequently generating the need for severe grinding, with high energy for use as anodic material.

The presence of potassium above 600 ppm and phosphorus above 200 ppm, even if it results in some improvement in the electrochemical performance of the battery, promotes serious problems in the preparation steps of the electrodes, due to resulting in mixed oxides of high hardness, with agglomerated particles. The excessive increase of potassium in the synthesis disqualifies the mixed oxide obtained as a potential anode material for lithium-ion batteries. The higher presence of phosphorus promotes the synthesis of niobium phosphates ($NbPO_5$ and $Nb_9PO_{25}$), with severe agglomerations of the particles.

The significant improvement in battery performance with the presence of tantalum, attributed to the formation of high-purity mixed oxide in $TiNb_2O_7$ and $TiTa_2O_7$, should be viewed with caution, due to the high cost of tantalum products, in the face of the need for low cost of future batteries and lithium ion for electric cars. However, it can be attractive for the production processes of mixed oxides, from ores with high concentrations of tantalum, which uses Ta-Nb separation, via the hydrofluoric acid process since fluoride does not promote problems in the synthesis of $TiNb_2O_7$. Due to the significant increase in battery performance obtained with the presence of tantalum, future scientific studies are recommended, with the approach of the optimal ratio between the mixed oxides $TiNb_2O_7$ and $TiTa_2O_7$ in the anodic material for future lithium-ion batteries.

## References

Aghamohammadi, H. (2022). A comprehensive review study on pure titanium niobium oxide as the anode material for Li-ion batteries. *Journal of Alloys and Compounds 911*.

Anix, C. (2016) Silicon-based anodes for lithium-ion batteries: Effectiveness of materials synthesis and electrode preparation, *Nano Energy, 27, 359-376.*

Barcellona, S. (2015). "Analysis of Ageing Effect on Li-Polymer Batteries". *The Scientific World Journal, 8.*

Bragal, N. d. (2007). Obtenção de titânio metálico com porosidade controlada por metalurgia do pó. *Química Nova 30.*

Bommier, C, & Ji X. (2018) Electrolytes, SEI Formation, and Binders: A Review of Nonelectrode Factors for Sodium-Ion Battery Anodes. *Small. 14(16)e1703576. 10.1002/smll.201703576.*

Bruziquesi, C. G. (2019). Nióbio: um elemento químico estratégico para o Brasil. *Quim. Nova,42(10), 1184-1188. org/10.21577/0100-4042.201*

Gielena, D. (2019). The role of renewable energy in the global energy transformation. *Energy Strategy Reviews, 38-50.*

Goodenough, J. B. (2014). Austin, TX (US). Patente Nº US 8,647,773 B2.

Griffith, J. K. (2020). Titanium Niobium Oxide: From Discovery to Application in Fast-Charging Lithium-Ion Batteries – *Chemistry of Materials, https://dx.doi.org/10.1021/acs.chemmater.0c02955 (2020). Chemistry of Materials. https://dx.doi.org/10.1021*

Hu, J. (2022). Effects of long-term fast charging on a layered cathode for lithium-ion batteries. *Journal of Energy Chemistry, volume 67, 604-612.*

Läubaum L., et al. (2020) Impact of Particle Size Distribution on Performance of Lithium-Ion Batteries, *GDCh Electrochemistry, 7(23), 4755-4766*

Lin, C. (2016). "Electrochemical and Mechanical Failure of Graphite-Based Anode Materials in Li-Ion Batteries for Electric Vehicles". *Journal of Chemistry. https: //doi.org/10.115*

Liu, G. (2018). Mesoporous $TiNb_2O_7$ microspheres as high-performance anode materials for lithium-ion batteries with high-rate capability and long cycle-life. *Electrochimica Acta 259, 20 - 27.*

Lou, J., & Wang, J. (2008). Nanomechanics and nanostructured multifunctional materials: Experiments, theories, and simulations. *Journal of Nanomaterials, 2008.*

Pereira A. S. et al. (2018). Metodologia da pesquisa científica. *UFSM.*

Rodríguez, O. (2020). Recovery of niobium and tantalum by solvent extraction from Sn–Ta–Nb mining tailings. *RSC Advances, 36.*

Takami, N. (2018). High-energy, fast-charging, long-life lithium-ion batteries using $TiNb_2O_7$ anodes for automotive applications. *Journal of Power Sources 396, 429–436.*

Wahyuningsih, S. (2017). $TiO_2$ Nanorods Preparation from Titanyl Sulphate. *Mater. Sci. Eng.*

Wang, J. (2020). Reductive Decomposition of Solvents and Additives toward Solid-Electrolyte Interphase Formation in Lithium-Ion Battery, *J. Phys. Chem.*

Weiss, M. (2021). Fast Charging of Lithium-Ion Batteries: A Review of Materials Aspects. *Jornal Advanced Energy Materials, 11, 2101126.*

Yang, C. (2016). Porous $TiNb_{24}O_{62}$ microspheres as high-performance anode materials for lithium-ion batteries of electric vehicles. *Royal Society of Chemistry, Nanoscale.*

Zhao, B R. R., Meilin Liu, Z. S. (2015) A comprehensive review of $Li_4Ti_5O_{12}$-based lectrodes for lithium-ion batteries: The latest advancements and future perspectives, *Materials Science and Engineering: R: Reports, 98, Pages 1-71, https://doi.org/10.1016/j.mser.2015.10.001*.